Resilient Dynamic State Estimation for Power System Using Cauchy-Kernel-Based Maximum Correntropy Cubature Kalman Filter

Yi Wang, *Member*, *IEEE*, Zhiwei Yang, Yaoqiang Wang, *Senior Member*, *IEEE*, Zhongwen Li, *Member*, *IEEE*, Venkata Dinavahi, *Fellow*, *IEEE*, and Jun Liang, *Senior Member* , *IEEE*

***Abstract*—Accurate estimation of dynamic states is the key to monitoring power system operating conditions and controlling transient stability. However, the inevitable non-Gaussian noise and randomly occurring denial-of-service (DoS) attacks may deteriorate the performance of standard filters seriously. To deal with these issues, a novel resilient cubature Kalman filter based on the Cauchy kernel maximum correntropy optimal criterion approach (termed CKMC-CKF) is developed, in which the Cauchy kernel function is utilized to describe the distance between vectors. Specifically, the errors of state and measurement in the cost function are unified by a statistical linearization technique, and the optimal estimated state is acquired by the fixed-point iteration method. Due to the salient thick-tailed feature and the insensitivity to the kernel bandwidth of Cauchy kernel function, the proposed CKMC-CKF can effectively mitigate the adverse effect of non-Gaussian noise and DoS attacks with a better numerical stability. Finally, the efficacy of the proposed method is demonstrated on the standard IEEE 39-bus system under various abnormal conditions. Compared with standard cubature Kalman filter (CKF) and maximum correntropy criterion CKF (MCC-CKF), the proposed algorithm reveals better estimation accuracy and stronger resilience.**

***Index Terms*—Dynamic state estimation, power system, resilience, maximum correntropy, non-Gaussian noise, DoS attacks.**

I. Introduction

With the widespread development of phasor measurement units (PMUs), dynamic state estimation (DSE) technology has been used to track hidden state variables of power system [1]-[3], such as node voltage amplitude, voltage phase angle, transient electromotive force of generators, etc. Indeed, synchronous generators are used to regulate generation interruption and load shedding with the change of power load [4], and the dynamic states of generators are used to enhance the stability of small signals. In fact, non-Gaussian heavy-tailed noise and network attacks (such as DoS) that occur at any time in the power system can seriously interfere with the dynamic state estimation of synchronous generators [5]. Therefore, in order to improve the anti-interference ability of synchronous generators under these abnormal conditions, it is of critical importance to develop some robust dynamic state estimation strategies for the stability of power systems.

For DSE, several methods based on the classical Kalman filter (KF) theory have been developed in the past several decades, such as extended KF (EKF) [6], unscented KF (UKF) [7], cubature KF (CKF) [8] and their extended versions [9]-[10], which aim to accurately track the internal state variables of synchronous generators. In view of the biased estimation that may be caused by the uncertain non-Gaussian process, an abridged Gaussian sum extended Kalman filter method was proposed in [11]. Considering the truncation error of EKF caused by the linearization approximation, several derivative-free DSE methodologies were designed. For example, by utilizing the square root UKF and the weighting factor acting on the measurement, [12] proposed a modified method to improve the numerical stability and robustness against measurement outliers. In [13], an adaptive UKF was introduced to simultaneously monitor the control input and status information of the integrated motor-transmission. By modeling the probability and distribution of attacks, an adaptive CKF based on variational Bayes was developed in [14], which can be utilized to estimate the states of randomly occurring injection attacks. There is no doubt that these previous research works have greatly enhanced the monitoring level of power system. However, it is worth pointing out that most of these previous approaches are developed utilizing objective functions with Gaussian noise distribution assumption. That is to say, these methods can only work well when the system and measurement noise strictly obey the Gaussian distribution. Therefore, the estimation performance of the approaches may deteriorate significantly in the presence of measurement outliers, such as the non-Gaussian noise and DoS attacks.

This work was supported in part by the National Natural Science Foundation of China under Grants 62203395 and 51507155, in part by the Postdoctoral Research Project of Henan Province under Grant 202101011, and in part by the Key R&D and Promotion Special Project of Henan Province under Grant Grants 222102520001 and 222102220041. (*Corresponding author: Yaoqiang Wang*.)

Yi Wang, Zhiwei Yang, Yaoqiang Wang, and Zhongwen Li are with the School of Electrical and Information Engineering, Zhengzhou University, Zhengzhou 450001, China, and also with the Henan Engineering Research Center of Power Electronics and Energy Systems, Zhengzhou 450001, China (e-mails: wangyi1414599008@163.com; 13253319984@163.com; WangyqEE@163.com; lzw@zzu.edu.cn).

Venkata Dinavahi is with the Department of Electrical and Computer Engineering, University of Alberta, Edmonton, AB T6G 2V4, Canada (e-mail: dinavahi@ualberta.ca).

Jun Liang is with the School of Electrical and Information Engineering, Zhengzhou University, Zhengzhou 450001, China, and also with the School of Engineering, Cardiff University, Cardiff CF24 3AA, UK. (e-mail: liangj1@cardiff.ac.uk).

In order to mitigate the adverse effects of outliers in the measurement function, such as non-Gaussian noise, load fluctuation [15] and cyber-attack [16]-[17], etc., several robust DSE strategies have been developed recently. For example, to diminish the estimation error caused by the malicious cyber-attacks, an estimation strategy based on distributed compressive sensing was constructed in [18]. Moreover, as a local similarity function of information theory learning (ITL), correntropy has excellent characteristics in dealing with non-Gaussian noise hypothesis because it contains the higher-order moments of probability density function. Among them, DSE algorithm based on maximum correntropy loss criterion is fused into classical EKF [19], UKF [20], which greatly enhances the robustness of standard Kalman filter against non-Gaussian noise. However, the optimal kernel bandwidth (KB) based on the maximum correntropy of Gaussian kernel is usually difficult to obtain in the real application, which needs a large number of experiments and debugging [20]. Thus, the practicability of the method maybe inevitably degraded. More importantly, the singular matrix issue appears in the Cholesky decomposition of Gaussian kernel function operation is also an urgent problem to be taken into account [21], which will seriously damage the calculation accuracy of DSE.

To deal with the aforementioned issues and improve the robustness of traditional DSEs against non-Gaussian noise and DoS attacks, based on the Cauchy kernel maximum correntropy optimal criterion, a novel resilient cubature Kalman filter is developed in the paper. The detailed contributions of this paper are threefold:

- Based on the Cauchy kernel maximum correntropy (CKMC), the developed CKMC-CKF method is insensitive to the kernel bandwidth, which can avoid extensive tests on the selection of optimal kernel bandwidth and improve efficiency.
- By utilizing the Cauchy kernel with two weighted local similarity functions to update the error and noise covariance, this greatly solves the problem of estimation accuracy degradation caused by non-Gaussian noise in the DSE process.
- By deducing a linear regression model with measurement loss probability, the robustness of the CKMC-CKF approach against DoS network attacks on measured data is effectively improved.

The remainder of this paper is organized as follows. Section II constructs the dynamic model of power system, the DoS attacks model, and then the maximum correntropy of Cauchy kernel theory are briefly introduced. Section III derives the resilient cubature Kalman filter based on the Cauchy kernel maximum correntropy optimal criterion. Section IV shows the numerical experimental results on the standard IEEE test system under various conditions. Finally, conclusions are drawn in Section V.

II. PROBLEM FORMULATION AND PRELIMINARIES

A. Dynamic Model of Power System

To track the dynamic states of power system, the power system model consisting of two nonlinear functions between state variables and measurements needs to be established, which can be expressed by

$$\begin{cases} \boldsymbol{x}_k = \boldsymbol{\phi}\left(\boldsymbol{x}_{k-1}, \boldsymbol{u}_{k-1}\right) + \boldsymbol{w}_{k-1}\,, & (1.a) \\ \boldsymbol{z}_k = \boldsymbol{h}\left(\boldsymbol{x}_k, \boldsymbol{u}_k\right) + \boldsymbol{v}_k\,, & (1.b) \end{cases}$$

where $\boldsymbol{\phi}(\cdot)$ and $\boldsymbol{h}(\cdot)$ represents the state propagation function and state measurement function, respectively; $\boldsymbol{x}_k$ and $\boldsymbol{z}_k$ denote the state variable and observation vector, respectively; $\boldsymbol{u}_k$ means the control input vector; $\boldsymbol{w}_{k-1}$ and $\boldsymbol{v}_k$ are respectively illustrate the system noise and measurement noise; the subscript k indicates the time scale.

In order to accurately track the status information of synchronous generator, the fourth-order model of a synchronous generator is adopted in this paper, which is closer to the actual operating mode of a generator than the traditional second-order generator model [23]. The state function of a generator can be established as follows [18]

$$\begin{cases} \dot{\delta} = \omega - \omega_0\,, & (2) \\ \dot{\omega} = \dfrac{\omega_0}{2T_j}\left[T_{\mathrm{m}} - T_{\mathrm{e}} - \dfrac{K_{\mathrm{D}}}{\omega_0}\left(\omega - \omega_0\right)\right], & (3) \\ \dot{e}_q^{'} = \dfrac{1}{T_{d0}^{'}}\left[E_{\mathrm{f}d} - e_q^{'} - \left(x_d - x_d^{'}\right) i_d\right], & (4) \\ \dot{e}_d^{'} = \dfrac{1}{T_{q0}^{'}}\left[-e_d^{'} + \left(x_q - x_q^{'}\right) i_q\right], & (5) \end{cases}$$

where δ, ω, $e_q^{'}$ and $e_d^{'}$ indicate the power angle, electrical angular velocity, transient electromotive force on q-axis and d-axis of a synchronous generator, respectively; ω_0 represents the initial value of ω; K_{D} indicates the damping factor; T_j, T_{m} and T_{e} are respectively denote the inertia constant, mechanical and electromagnetic power; $E_{\mathrm{f}d}$ means the excitation voltage of stator; x_d, $x_d^{'}$, x_q and $x_q^{'}$ are respectively symbolize the synchronous and transient reactance of generator's d-axis and q-axis; $T_{d0}^{'}$, $T_{q0}^{'}$, i_d and i_q indicate the d and q axis time constants and stator currents, respectively.

In this study, by contrast with equation (1.a), the state variable is set as $\boldsymbol{x}_k = [\delta,\ \omega,\ e_q^{'},\ e_d^{'}]^T$, and the control input vector is $\boldsymbol{u}_k = [T_m,\ E_{fd},\ i_R,\ i_I]^T$. To improve the state estimation accuracy, the measurement with a higher redundancy is utilized, which is set as $\boldsymbol{z}_k = [\delta,\ \omega,\ e_R,\ e_I]^T$; where e_R and e_I are given by

$$e_R = \left(e_d^{'} + i_d x_q^{'}\right)\sin(\delta) + \left(e_q^{'} - i_d x_d^{'}\right)\cos(\delta)\,, \quad (6)$$

$$e_I = \left(e_q^{'} - i_d x_d^{'}\right)\sin(\delta) - \left(e_d^{'} + i_q x_q^{'}\right)\cos(\delta)\,, \quad (7)$$

In addition, in order to facilitate the solution, i_d and i_q in the above formulas need to be further expressed as functions of state variables and input variables, which are given by

$$i_d = i_R \sin(\delta) - i_I \cos(\delta)\,, \quad (8)$$

$$i_q = i_I \sin(\delta) + i_R \cos(\delta)\,. \quad (9)$$

B. Model of DoS Attacks

With the gradual application of power grid intelligence, the actual power data is often subject to cyber-attack [24]-[26], especially for the frequent DoS attacks, which will inevitably lead to the loss of the measurement taken from the PMU. Obviously, the DoS attacks can result in erroneous estimation result.

To depict the mechanics of DoS attacks, a series of data sets $\{u_k\}$ $(k=1,2,...,m)$ are adopted to model the loss of measurement data caused by DoS attacks, which are described by Bernoulli distribution and expressed as follows

$$u_k = \begin{cases} 1 \\ 0 \end{cases}, \tag{10}$$

$$\begin{aligned} \mathrm{var}(u_k = 1) &= \boldsymbol{P}_s(u_k = 0) \cdot \boldsymbol{P}_s(u_k = 1) \\ &= \rho \cdot (1-\rho) \end{aligned}. \tag{11}$$

where ρ is the probability of measurement loss, $0 \le \rho \le 1$. When $u_k = 1$, it means there was no DoS attacks on the measurement data; otherwise, when $u_k = 0$, it indicates that the measurement data has been subjected to DoS attacks, and the measurements are incomplete.

Therefore, the real measurement information collected by PMU under DoS attacks can be modeled by

$$\boldsymbol{Z}_k^{'} = u_k \times \boldsymbol{Z}_k \quad k=1,2,...,m\,. \tag{12}$$

C. Cauchy Kernel Maximum Correntropy

As a measure of statistical similarity, the correntropy can be defined by two random variables $\boldsymbol{X}$ and $\boldsymbol{Y}$ as follows [27]:

$$\boldsymbol{V}(\boldsymbol{X},\boldsymbol{Y}) = \boldsymbol{E}\left[\kappa_\sigma(\boldsymbol{X},\boldsymbol{Y})\right] = \int \kappa_\sigma(\boldsymbol{x},\boldsymbol{y})\ f_{x,y}(\boldsymbol{x},\boldsymbol{y})\ dxdy \tag{13}$$

where $\boldsymbol{E}(\cdot)$ means the expectation operator, $\kappa_\sigma(\cdot)$ is the Mercer kernel of the correntropy, and the kernel bandwidth is σ. $f_{x,y}(\boldsymbol{x},\boldsymbol{y})$ represents the joint probability density function (PDF) between $\boldsymbol{x}$ and $\boldsymbol{y}$. Due to the inaccessibility of $f_{x,y}(\boldsymbol{x},\boldsymbol{y})$ and the limitation of sample, (13) can be approximately estimated by

$$\widehat{\boldsymbol{V}}(\boldsymbol{X},\boldsymbol{Y}) = \frac{1}{N}\sum_{i=1}^{N} \kappa_\sigma(\boldsymbol{x}_k,\boldsymbol{y}_k)\,. \tag{14}$$

In the information theoretic learning (ITL), the Gaussian kernel is often regarded as a kernel function of correntropy. In this paper, a Cauchy kernel is utilized as the kernel function of correntropy, which is insensitive to the kernel bandwidth compared to the Gaussian kernel [28]. The Cauchy kernel function is defined as follows

$$C_\sigma(e) = \frac{1}{1+e^2/\sigma}, \tag{15}$$

where $e = x - y$, $C_\sigma(\cdot)$ denotes a Cauchy kernel of the correntropy, σ symbolizes the kernel bandwidth ($\sigma > 0$).

By maximizing (14) and combining with (15), a cost function based on the Cauchy-kernel-based maximum correntropy (named CKMC) can be expressed by:

$$J_{CKMC} = \frac{1}{N}\sum_{i=1}^{N} \boldsymbol{C}_\sigma(\boldsymbol{x}_k,\boldsymbol{y}_k)\,. \tag{16}$$

III. Derivation of the Proposed CKMC-CKF Method

In this section, the resilient cubature Kalman filter based on Cauchy kernel maximum correntropy criterion (named CKMC-CKF) is derived in detail. The proposed CKMC-CKF method is mainly containing the three consecutive parts: (1) time update; (2) measurement update; (3) derivation of linear regression model.

A. Time Update

(1) ***Initialization***: when k=0, the initial mean and covariance matrix of the state variables $\{\boldsymbol{X}_i\}(i=1,2,...,n)$ can be obtained by

$$\widehat{\boldsymbol{X}}_{0|0} = \boldsymbol{E}\left[\boldsymbol{X}_0\right], \tag{17}$$

$$\boldsymbol{P}_{0|0} = \boldsymbol{E}\left[\left(\boldsymbol{X}_0 - \widehat{\boldsymbol{X}}_{0|0}\right)\left(\boldsymbol{X}_0 - \widehat{\boldsymbol{X}}_{0|0}\right)^{\mathrm{T}}\right]. \tag{18}$$

(2) ***State Prediction***: when $k > 0$, by utilizing the state mean value and covariance matrix at time instant $k-1$, a priori estimate of the state variable and its covariance can be obtained.

In the first place, based on the spherical-radial cubature rule, a set of cubature points can be generated by

$$\boldsymbol{P}_{k-1|\,k-1} = \boldsymbol{S}_{k-1|\,k-1}\boldsymbol{S}_{k-1|\,k-1}^{\mathrm{T}}, \tag{19}$$

$$\boldsymbol{X}_{i,k-1|\,k-1} = \boldsymbol{S}_{k-1|\,k-1}\boldsymbol{\xi}_i + \widehat{\boldsymbol{X}}_{k-1|\,k-1}, \quad \text{for } i=1,\ldots,2n\,, \tag{20}$$

where $\boldsymbol{S}_{k-1|\,k-1}$ can be achieved by Cholesky decomposition of $\boldsymbol{P}_{k-1|\,k-1}$; $\{\boldsymbol{\xi}_i\}(i=1,2,...,2n)$ is defined as

$$\boldsymbol{\xi}_i = \begin{cases} \boldsymbol{e}_i & i=1,2,...,n \\ -\boldsymbol{e}_i & i=n+1,n+2,...,2n \end{cases}, \tag{21}$$

where $\boldsymbol{e}_i \in \mathbb{R}^{n\times n}$ represents the identity matrix.

After the cubature point $\boldsymbol{X}_{i,k-1|\,k-1}$ is propagated through the state function $\phi(\cdot)$, (20) can be transformed into

$$\boldsymbol{X}_{i,k|\,k-1}^{*} = \phi\left(\boldsymbol{X}_{i,k-1|\,k-1}, \boldsymbol{u}_k\right). \tag{22}$$

By utilizing the cubature points $\boldsymbol{X}_{i,k|\,k-1}^{*}$, the prediction of state variables and covariance matrix can be calculated by

$$\widehat{\boldsymbol{X}}_{k|\,k-1} = \frac{1}{2n}\sum_{i=1}^{2n} \boldsymbol{X}_{i,k|\,k-1}^{*}\,, \tag{23}$$

$$\boldsymbol{P}_{k|\,k-1} = \frac{1}{2n}\sum_{i=1}^{2n} \mathbf{X}_{i,k|\,k-1}^{*}(\mathbf{X}_{i,k|\,k-1}^{*})^{T} - \widehat{\mathbf{X}}_{k|\,k-1}\widehat{\mathbf{X}}_{k|\,k-1}^{T} + \mathbf{Q}_{k-1}. \tag{24}$$

where $\boldsymbol{Q}_{k-1}$ represents the process noise covariance matrix at the time instant $k-1$.

B. Measurement Update

Likewise, based on the state prediction above, a set of equal-weight cubature points $\boldsymbol{X}_{i,k|\,k-1}$ is generated by

$$\boldsymbol{P}_{k|\,k-1} = \boldsymbol{S}_{k|\,k-1}\boldsymbol{S}_{k|\,k-1}^{\mathrm{T}}, \tag{25}$$

$$\boldsymbol{X}_{i,k|\,k-1} = \boldsymbol{S}_{k|\,k-1}\boldsymbol{\xi}_i + \widehat{\boldsymbol{X}}_{k|\,k-1}, \quad \text{for } i=1,\ldots,2n\,. \tag{26}$$

After being propagated by the measured function $\boldsymbol{h}(\cdot)$, the cubature points are deformed as

$$\boldsymbol{Z}_{i,k|k-1} = u_k \cdot \boldsymbol{h}\left(\boldsymbol{X}_k^{\boldsymbol{m}}, \boldsymbol{X}_{i,k|k-1}\right). \tag{27}$$

Note that the measured packet loss coefficient u_k is considered here, which is different from the traditional CKF procedure.

Subsequently, the mean values $\widehat{\boldsymbol{Z}}_{k|k-1}$ and cross-covariance $\boldsymbol{P}_{xz,k|k-1}$ for measurements can be further developed by

$$\widehat{\boldsymbol{Z}}_{k|k-1} = \frac{1}{2n}\sum_{i=1}^{2n} \boldsymbol{Z}_{i,k|k-1}, \tag{28}$$

$$\boldsymbol{P}_{xz,k|k-1} = \frac{1}{2n}\sum_{i=1}^{2n} \boldsymbol{X}_{i,k|k-1}\boldsymbol{Z}_{i,k|k-1}^{T} - \widehat{\boldsymbol{X}}_{k|k-1}\widehat{\boldsymbol{Z}}_{k|k-1}^{T}. \tag{29}$$

C. Derivation of Linear Regression Model

To facilitate matrix solution, a measurement slope matrix is defined as $\boldsymbol{H}_k = (\boldsymbol{P}_{k|k-1}^{-1}\boldsymbol{P}_{xz,k|k-1})^{\boldsymbol{T}}$, by linear approximation to the measurement function $\boldsymbol{h}(\cdot)$, then (1.b) under DoS attacks can be further transformed into

$$\boldsymbol{Z}_k^{'} = \widehat{\boldsymbol{Z}}_{k|k-1} + \boldsymbol{H}_k(\boldsymbol{X}_k - \widehat{\boldsymbol{X}}_{k|k-1}) + \boldsymbol{v}_k. \tag{30}$$

Note that the packet loss factor u_k is taken into account in $\boldsymbol{Z}_k^{'}$ here. By combining (1.a) and (30), a linear regression model for $\boldsymbol{X}_k$ is further evolved as follows

$$\begin{bmatrix} \widehat{\boldsymbol{X}}_{k|k-1} \\ \boldsymbol{Z}_k^{'} - \widehat{\boldsymbol{Z}}_{k|k-1} + \boldsymbol{H}_k\widehat{\boldsymbol{X}}_{k|k-1} \end{bmatrix} = \begin{bmatrix} \boldsymbol{I} \\ \boldsymbol{H}_k \end{bmatrix}\boldsymbol{X}_k + \xi_k, \tag{31}$$

where $\boldsymbol{\xi}_k$ represents the error vector with respect to the states and measurements as

$$\boldsymbol{\xi}_k = \begin{bmatrix} -(\boldsymbol{X}_k - \widehat{\boldsymbol{X}}_{k|k-1}) \\ \boldsymbol{v}_k \end{bmatrix}. \tag{32}$$

Also,

$$\boldsymbol{E}\left[\xi_k \xi_k^{\mathrm{T}}\right] = \begin{bmatrix} \boldsymbol{P}_{k|k-1} & 0 \\ 0 & \boldsymbol{R}_k \end{bmatrix} = \begin{bmatrix} \boldsymbol{B}_{p,k|k-1}\boldsymbol{B}_{p,k|k-1}^{\mathrm{T}} & 0 \\ 0 & \boldsymbol{B}_{r,k}\boldsymbol{B}_{r,k}^{\mathrm{T}} \end{bmatrix}. \tag{33}$$

where $\boldsymbol{B}_{p,k|k-1}$ and $\boldsymbol{B}_{r,k}$ are the Cholesky decomposition factors of $\boldsymbol{P}_{k|k-1}$ and $\boldsymbol{R}_k$, respectively.

Based on equation (16), the optimal cost function of the CKF algorithm based on the CKMC criterion can be refined as

$$J_{\mathrm{CKMC}} = \frac{1}{n+m}\left[\sum_{i=1}^{n} C_\sigma(\boldsymbol{e}_{x,i}) + \sum_{i=1}^{m}(C_\sigma \boldsymbol{e}_{z,i})\right], \tag{34}$$

where n and m respectively represent the dimensions of states and measurements. Simultaneously, the difference $\boldsymbol{e}_{x,i}$ and $\boldsymbol{e}_{z,i}$ are given by

$$\boldsymbol{e}_{x,i} = \boldsymbol{B}_{p,k|k-1}^{-1}(\boldsymbol{X}_k - \widehat{\boldsymbol{X}}_{k|k-1}), \tag{35}$$

$$\boldsymbol{e}_{z,i} = \boldsymbol{B}_{r,k}^{-1}(\boldsymbol{Z}_k^{'} - \widehat{\boldsymbol{Z}}_{k|k-1} - \boldsymbol{H}_k(\boldsymbol{X}_k - \widehat{\boldsymbol{X}}_{k|k-1})). \tag{36}$$

In order to solve the optimal state, by taking the partial derivative of (34) and let $\partial J_{\mathrm{CKMC}} / \partial X_k = 0$, which is calculated by

$$\begin{aligned} &\sum_{i=1}^{n} C_\sigma^2(\boldsymbol{e}_{x,i})\boldsymbol{B}_{p,k|k-1}^{-T}\boldsymbol{B}_{p,k|k-1}^{-1}(\boldsymbol{X}_k - \widehat{\boldsymbol{X}}_{k|k-1}) \\ &-\sum_{i=1}^{m} C_\sigma^2(\boldsymbol{e}_{z,i})\boldsymbol{H}_k^T\boldsymbol{B}_{r,k}^{-T}\boldsymbol{B}_{r,k}^{-1}(\boldsymbol{Z}_k^{'} - \widehat{\boldsymbol{Z}}_{k|k-1} - \boldsymbol{H}_k(\boldsymbol{X}_k - \widehat{\boldsymbol{X}}_{k|k-1})) = 0 \end{aligned}, \tag{37}$$

Eq. (37) can be further simplified as

$$\begin{aligned} &\boldsymbol{B}_{p,k|k-1}^{-T}\boldsymbol{U}_x\boldsymbol{B}_{p,k|k-1}^{-1}(\boldsymbol{X}_k - \widehat{\boldsymbol{X}}_{k|k-1}) - \\ &\boldsymbol{H}_k^T\boldsymbol{B}_{r,k}^{-T}\boldsymbol{U}_z\boldsymbol{B}_{r,k}^{-1}(\boldsymbol{Z}_k^{'} - \widehat{\boldsymbol{Z}}_{k|k-1} - \boldsymbol{H}_k(\boldsymbol{X}_k - \widehat{\boldsymbol{X}}_{k|k-1})) = 0 \end{aligned}, \tag{38}$$

where

$$\boldsymbol{U}_x = diag\left(C_\sigma^2(\boldsymbol{e}_{x,1}), \ldots, C_\sigma^2(\boldsymbol{e}_{x,n})\right), \tag{39}$$

$$\boldsymbol{U}_z = diag\left(C_\sigma^2(\boldsymbol{e}_{z,1}), \ldots, C_\sigma^2(\boldsymbol{e}_{z,m})\right), \tag{40}$$

Next, let

$$\widetilde{\boldsymbol{P}}_{k|k-1} = \boldsymbol{B}_{p,k|k-1}^{-T}\boldsymbol{U}_x\boldsymbol{B}_{p,k|k-1}^{-1}, \tag{41}$$

$$\widetilde{\boldsymbol{R}}_k = \boldsymbol{B}_{r,k}^{-T}\boldsymbol{U}_z\boldsymbol{B}_{r,k}^{-1}. \tag{42}$$

Then, Eq. (38) is further transformed into the form as

$$(\widetilde{\boldsymbol{P}}_{k|k-1}^{-1} + \boldsymbol{H}_k^T\widetilde{\boldsymbol{R}}_k^{-1}\boldsymbol{H}_k)\boldsymbol{X}_k = \widetilde{\boldsymbol{P}}_{k|k-1}^{-1}\widehat{\boldsymbol{X}}_{k|k-1} + \boldsymbol{H}_k^T\widetilde{\boldsymbol{R}}_k^{-1}\boldsymbol{Z}_k^{'}. \tag{43}$$

Add and subtract $\boldsymbol{H}_k^T\widetilde{\boldsymbol{R}}_k^{-1}\boldsymbol{H}_k\widehat{\boldsymbol{X}}_{k|k-1}$ on the right side of (43), it yields

$$\begin{aligned} (\widetilde{\boldsymbol{P}}_{k|k-1}^{-1} + \boldsymbol{H}_k^T\widetilde{\boldsymbol{R}}_k^{-1}\boldsymbol{H}_k)\boldsymbol{X}_k = &(\widetilde{\boldsymbol{P}}_{k|k-1}^{-1} + \boldsymbol{H}_k^T\widetilde{\boldsymbol{R}}_k^{-1}\boldsymbol{H}_k)\widehat{\boldsymbol{X}}_{k|k-1} \\ &+ \boldsymbol{H}_k^T\widetilde{\boldsymbol{R}}_k^{-1}(\boldsymbol{Z}_k^{'} - \widehat{\boldsymbol{Z}}_{k|k-1}) \end{aligned}. \tag{44}$$

Note that $(\widetilde{\boldsymbol{P}}_{k|k-1}^{-1} + \boldsymbol{H}_k^T\widetilde{\boldsymbol{R}}_k^{-1}\boldsymbol{H}_k)$ is positive definite here. Further, (44) is evolved as

$$\boldsymbol{X}_k = \widehat{\boldsymbol{X}}_{k|k-1} + \boldsymbol{K}_k(\boldsymbol{Z}_k^{'} - \widehat{\boldsymbol{Z}}_{k|k-1}). \tag{45}$$

where the gain matrix $\boldsymbol{K}_k$ can be derived as

$$\begin{aligned} \boldsymbol{K}_k &= (\widetilde{\boldsymbol{P}}_{k|k-1}^{-1} + \boldsymbol{H}_k^T\widetilde{\boldsymbol{R}}_k^{-1}\boldsymbol{H}_k)^{-1}\boldsymbol{H}_k^T\widetilde{\boldsymbol{R}}_k^{-1} \\ &= \widetilde{\boldsymbol{P}}_{k|k-1}\boldsymbol{H}_k^T(\boldsymbol{H}_k\widetilde{\boldsymbol{P}}_{k|k-1}\boldsymbol{H}_k^T + \widetilde{\boldsymbol{R}_k})^{-1} \end{aligned}. \tag{46}$$

Therefore, the posterior error covariance $\boldsymbol{P}_{k|k}$ with respect to the state variables $\boldsymbol{X}_k$ is obtained as

$$\boldsymbol{P}_{k|k} = \widetilde{\boldsymbol{P}}_{k|k-1} - \boldsymbol{K}_k\boldsymbol{P}_{zz,k|k-1}\boldsymbol{K}_k^{\mathrm{T}}. \tag{47}$$

Remark 1: To enhance the robustness of DSE method against non-Gaussian noise or DoS attacks, some modified methods have been developed. However, it's worth pointing out that most of the existing methods are based on the maximum correntropy criterion that utilizes the Gaussian kernel [19]. These approaches have the following obvious shortcomings. On the one hand, it is difficult to select the optimal KB, which needs to be obtained through multiple experiments. On the other hand, the singular matrix problem often occurs when the Gaussian kernel function is calculated by Cholesky decomposition [21]. Therefore, these methods based on maximum correntropy of the Gaussian kernel can not satisfy the requirement of dynamic state estimation in the rapidity and reliability.

Remark 2: Compared with the DSE methods based on the Gaussian kernel in [19], [21], the proposed resilient CKMC-CKF approach that utilize the Cauchy kernel maximum correntropy with weighted local similarities is not only able to effectively avoid the singularity of Cholesky decomposition, but also insensitive to the KB. Therefore, the CKMC-CKF method can achieve a stronger robustness and restrain the influence of outliers on the accuracy of state estimation effectively.

Finally, to find the optimal states in (44), an iterative algorithm can be utilized to deal with the nonlinearity of states $\boldsymbol{X}_k$ in (44), the detailed steps are summarized in TABLE I.

TABLE I
PROCEDURE OF THE CKMC-CKF

Algorithm 1

Step 1: Set k=0, $\widehat{\boldsymbol{X}}_{0|0}$, $\widehat{\boldsymbol{P}}_{0|0}$, $\boldsymbol{Q}_{k-1}$, $\boldsymbol{R}_k$

Step 2: Calculate $\widehat{\boldsymbol{X}}_{k|k-1}$ and $\boldsymbol{P}_{k|k-1}$ by Eq. (23)-(24)

Step 3: Calculate $\widehat{\boldsymbol{Z}}_{k|k-1}$ and $\boldsymbol{P}_{xz,k|k-1}$ by Eq. (28)-(29)

Step 4: Set $j=1$, $\widehat{\boldsymbol{X}}_{k|k}^{(0)}=\widehat{\boldsymbol{X}}_{k|k-1}$

Step 5: Update $\widehat{\boldsymbol{X}}_{k|k}^{(j)}$ and $\boldsymbol{P}_{k|k}^{(j)}$ by Eq. (43)-(45)

$$\boldsymbol{K}_k^{(j-1)}=\widetilde{\boldsymbol{P}}_{k|k-1}^{(j-1)}\boldsymbol{H}_k^{T}(\boldsymbol{H}_k\widetilde{\boldsymbol{P}}_{k|k-1}^{(j-1)}\boldsymbol{H}_k^{T}+\widetilde{\boldsymbol{R}}_k^{(j-1)})^{-1}$$

$$\widehat{\boldsymbol{X}}_{k|k}^{(j)}=\widehat{\boldsymbol{X}}_{k|k-1}+\boldsymbol{K}_k^{(j-1)}(\boldsymbol{Z}_k^{'}-\widehat{\boldsymbol{Z}}_{k|k-1})$$

$$\boldsymbol{P}_{k|k}^{(j)}=\widetilde{\boldsymbol{P}}_{k|k-1}^{(j-1)}-\boldsymbol{K}_k^{(j-1)}\boldsymbol{P}_{zz,k|k-1}(\boldsymbol{K}_k^{(j-1)})^{T}$$

where, calculate $\widetilde{\boldsymbol{P}}_{k|k-1}^{(j-1)}$ and $\widetilde{\boldsymbol{R}}_k^{(j-1)}$ by Eq. (34) and Eq. (37)

$$\widetilde{\boldsymbol{P}}_{k|k-1}^{(j-1)}=\boldsymbol{B}_{p,k|k-1}^{-T}\boldsymbol{U}_x^{(j-1)}\boldsymbol{B}_{p,k|k-1}^{-1}$$

$$\widetilde{\boldsymbol{R}}_k^{(j-1)}=\boldsymbol{B}_{r,k}^{-T}\boldsymbol{U}_z^{(j-1)}\boldsymbol{B}_{r,k}^{-1}$$

$$\boldsymbol{e}_{x,i}^{(j-1)}=\boldsymbol{B}_{p,k|k-1}^{-1}(\widehat{\boldsymbol{X}}_{k|k}^{(j)}-\widehat{\boldsymbol{X}}_{k|k-1})$$

$$\boldsymbol{e}_{z,i}^{(j-1)}=\boldsymbol{B}_{r,k}^{-1}(\boldsymbol{Z}_k^{'}-\widehat{\boldsymbol{Z}}_{k|k-1}-\boldsymbol{H}_k(\widehat{\boldsymbol{X}}_{k|k}^{(j-1)}-\widehat{\boldsymbol{X}}_{k|k-1}))$$

with

$$\boldsymbol{U}_x^{(j-1)}=diag\left(C_\sigma^2\left(\boldsymbol{e}_{x,1}^{(j-1)}\right),\ldots,C_\sigma^2\left(\boldsymbol{e}_{x,n}^{(j-1)}\right)\right)$$

$$\boldsymbol{U}_z^{(j-1)}=diag\left(C_\sigma^2\left(\boldsymbol{e}_{z,1}^{(j-1)}\right),\ldots,C_\sigma^2\left(\boldsymbol{e}_{z,m}^{(j-1)}\right)\right)$$

Step 6: Set $j=j+1$

Until $\dfrac{\left\|\widehat{\boldsymbol{X}}_{k|k}^{(j)}-\widehat{\boldsymbol{X}}_{k|k}^{(j-1)}\right\|}{\left\|\widehat{\boldsymbol{X}}_{k|k}^{(j-1)}\right\|}\le\varepsilon$ holds, set $\widehat{\boldsymbol{X}}_{k|k}=\widehat{\boldsymbol{X}}_{k|k}^{(j)}$,

$\boldsymbol{P}_{k|k}=\boldsymbol{P}_{k|k}^{(j)}$

End

Step 7: $k=k+1$, go back to ***Step 2***.

IV. NUMERICAL RESULTS

In this section, the IEEE standard system with ten-generator thirty-nine buses [30] is utilized to mimic the response of the real power system, which is sampled by the PMU device. To be specific, the sampling frequency of measurement is 50. Due to the randomness of the noise distribution, the Monte-Carlo (MC) sampling method is used to mimic the statistical information of the random noise distribution, and $N_{MC}=200$ is set here, which is implemented in the simulation experiments of each subsequent example. At $t=0.5\,s$, a large system disturbance to the three-phase ground fault occurs on the bus 16-21, which is removed at $t=0.7\,s$. Assume that the state variable $\widehat{\boldsymbol{X}}_{0|0}$ is initialized to the steady state operating values and the initial error covariance $\widehat{\boldsymbol{P}}_{0|0}=10^{-5}$. In addition, the noise covariance matrix (i.e., $\boldsymbol{Q}_k$ and $\boldsymbol{R}_k$) for the process and measurement is set to 10^{-5} and 10^{-6}, respectively. Taking the synchronous generator G2 as an example randomly, the cubature Kalman filtering (CKF) and maximum correntropy criterion cubature Kalman filtering (MCC-CKF) [22] are also exploited to compare with the proposed approach, which aims to highlight the effectiveness of the proposed CKMC-CKF algorithm. In addition, all test environments are based on Intel Core TM i5 2.30-GHz CPU with 16-GB memory computer.

Based on the MC sampling, two types of error values are utilized to assess the estimation performance of different DSE algorithms [30], which are defined as follows

$$MAE(k)=\frac{1}{N_{MC}}\sum_{i=1}^{N_{MC}}\frac{1}{N_S}\sum_{i=1}^{N_S}\left|\boldsymbol{X}_{i,k}-\widehat{\boldsymbol{X}}_{i,k}\right|, \tag{48}$$

$$O_x=\frac{1}{N_{MC}}\sum_{i=1}^{N_{MC}}\sqrt{\sum_{k=1}^{N_T}\left(\boldsymbol{X}_{i,k}-\widehat{\boldsymbol{X}}_{i,k}\right)^2/N_T}\,. \tag{49}$$

where $MAE(k)$ is the mean absolute error, O_x represents the overall performance error; $\boldsymbol{X}_{i,k}$ and $\widehat{\boldsymbol{X}}_{i,k}$ are respectively denoting the true states and estimated states at the time instant k. N_{MC}, N_S and N_T are the total number of MC trials, state variables and simulation steps, respectively. Based on literature [23] and [30], the permitted range of the two error indicators should be less than 0.25 and 0.5 respectively.

A. Different Kernel Bandwidth Tests

As stated in [19], different kernel bandwidths (KB) in correntropy have decisive significance for the accuracy of state estimation. To be specific, a KB that is too large may not be able to suppress outliers, while a KB that is too small may also lead to slow convergence, both of which prove that the choice of kernel bandwidths needs to be careful for the robustness of DSE. TABLE II presents the error performance metrics of the proposed CKMC-CKF algorithm under different kernel bandwidths.

TABLE II
ERROR PERFORMANCE METRICS OF CKMC-CKF WITH DIFFERENT KERNEL BANDWIDTH

Kernel bandwidth (σ)	$MAE(k)$	O_x
$\sigma=20$	1.43×10^{-3}	1.98×10^{-3}
$\sigma=30$	1.41×10^{-3}	1.94×10^{-3}
$\sigma=50$	1.40×10^{-3}	1.94×10^{-3}
$\sigma=80$	1.41×10^{-3}	1.95×10^{-3}
$\sigma=100$	1.40×10^{-3}	1.95×10^{-3}

It can be found from the results that the estimation errors of CKMC-CKF method with different KBs are not much different. This is because the correntropy loss criterion based

on the Cauchy kernel is not sensitive to the selection of kernel bandwidths, which can avoid numerous experiments for acquiring the appropriate value of KB. Thus, the generality of the proposed algorithm can be improved. For ease of description, the KB of CKMC-CKF is set as $\sigma = 50$, which is used in subsequent tests.

B. Unknown Gaussian Noise Test

Due to the variability of operating conditions, the statistical characteristics of noise (i.e., $\boldsymbol{Q}_k$ and $\boldsymbol{R}_k$) will vary over time in the actual power system [30]. In other words, the actual noise is unknown. To verify the performance of the proposed method in this case, the covariance of process noise and measurement noise is set as $\boldsymbol{Q}_k = \mathrm{diag}[10^{-3}, 10, 10^{-1}, 10^{-1}]$, $\boldsymbol{R}_k = \mathrm{diag}[10^{-5}, 10^{-5}, 10^{-3}, 10^{-5}]$, respectively. Meanwhile, the KB of MCC-CKF is set to 10.

In this scenario, the standard CKF, the MCC-CKF method, and the developed CKMC-CKF approach are implemented for comparison. The state estimation results of different filtering methodologies are depicted in Fig. 1, where p.u. represents the standard unit value. It can be seen that the CKF has the largest estimation error for the state variable tracking of the synchronous generator, especially the state e_d'. Followed by the MCC-CKF, which is somewhat resistant to uncertain Gaussian noise. However, MCC-CKF is also limited due to its reliance on KB. Compared with CKF and MCC-CKF methods, the developed CKMC-CKF can achieve the fastest tracking speed for real states on account of its insensitivity to different kernel bandwidths, therefore, the CKMC-CKF can outperform the standard CKF and MCC-CKF method.

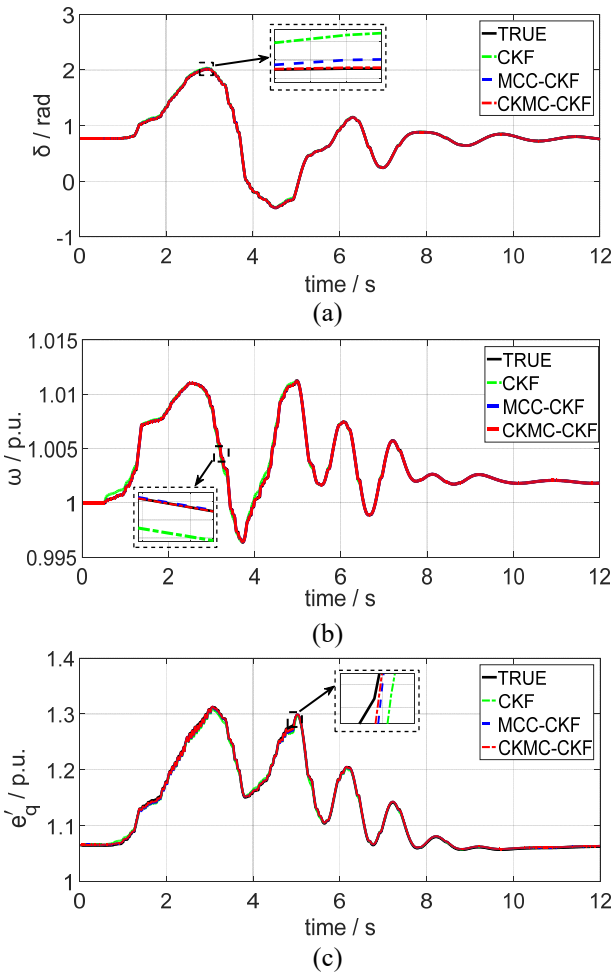

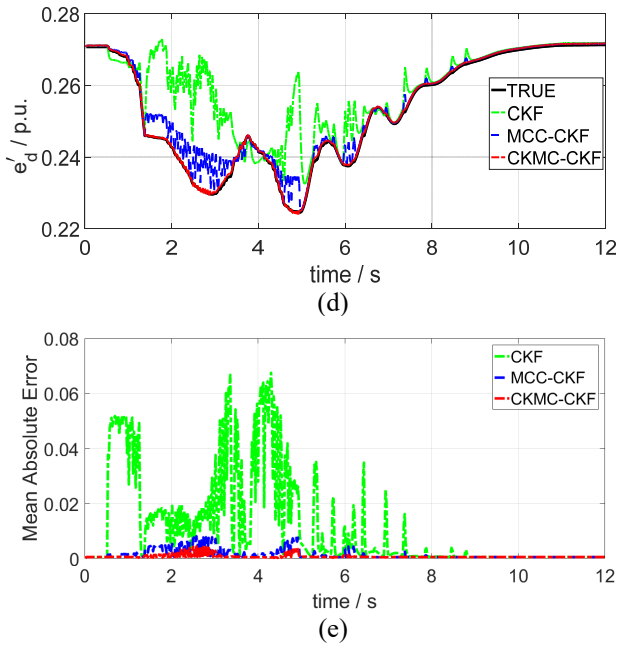

Fig. 1 Estimation performance of the CKF, the MCC-CKF and the CKMC-CKF with unknown Gaussian noise. (a) state δ, (b) state ω, (c) state e_q', (d) state e_d', (e) MAE results.

In addition, the estimation error metrics of all the discussed approaches for different state variables are presented in the Table III, which clearly conclude that the filtering performance of CKF is the worst because its two estimation error indicators ($MAE(k)$ and O_x) are the largest, followed by MCC-CKF, and that of CKMC-CKF is the smallest. These results further confirm the efficiency of the developed CKMC-CKF method in this occasion.

TABLE III
ESTIMATION ERROR METRICS OF DIFFERENT METHODS WITH UNKNOWN GAUSSIAN NOISE

States	CKF		MCC-CKF		CKMC-CKF	
	O_x	$MAE(k)$	O_x	$MAE(k)$	O_x	$MAE(k)$
δ	0.0054	0.0029	0.0019	0.0009	0.0002	0.0001
ω	0.0401	0.0209	0.0011	0.0006	0.0001	0.0003
e_q'	0.0028	0.0019	0.0024	0.0015	0.0019	0.0014
e_d'	0.0079	0.0044	0.0032	0.0017	0.0004	0.0004

C. Non-Gaussian Noise Test

For the actual power system, the distribution of system noise and measurement noise may not obey the Gaussian strictly [10]. To verify the effectiveness of the developed approach in this condition, the measurement noise is assumed as a Gaussian mixture, which is defined and generated by

$$r_k \sim (1-\theta)N\left(0, v_1^2\right) + \theta N\left(0, v_2^2\right), \tag{50}$$

where $N(0,v_i^2)$ represents the Gaussian distribution with a zero mean and a covariance of $v_i^2(i=1,2)$; θ represents the coefficient of mixture.

Fig. 2 shows the estimate results of several discussed filter algorithms when $\theta=0.9$. It can be seen from Fig. 2, we can find that the estimation accuracy of CKF based on Gaussian noise assumption is reduced seriously. Compared with traditional CKF, the MCC-CKF method based on Gaussian kernel can achieve a better tracking speed, however, in view of the limitation that it can only deal with certain types of non-Gaussian noise, and the singularity may occur in the Cholesky decomposition process of the matrixes, there is still a large estimation error. Furthermore, as predicted by the theoretical analysis, the developed CKMC-CKF approach owns the best estimation accuracy, this is because that it is utilizing the Cauchy kernel with two kinds of weighted local similarity.

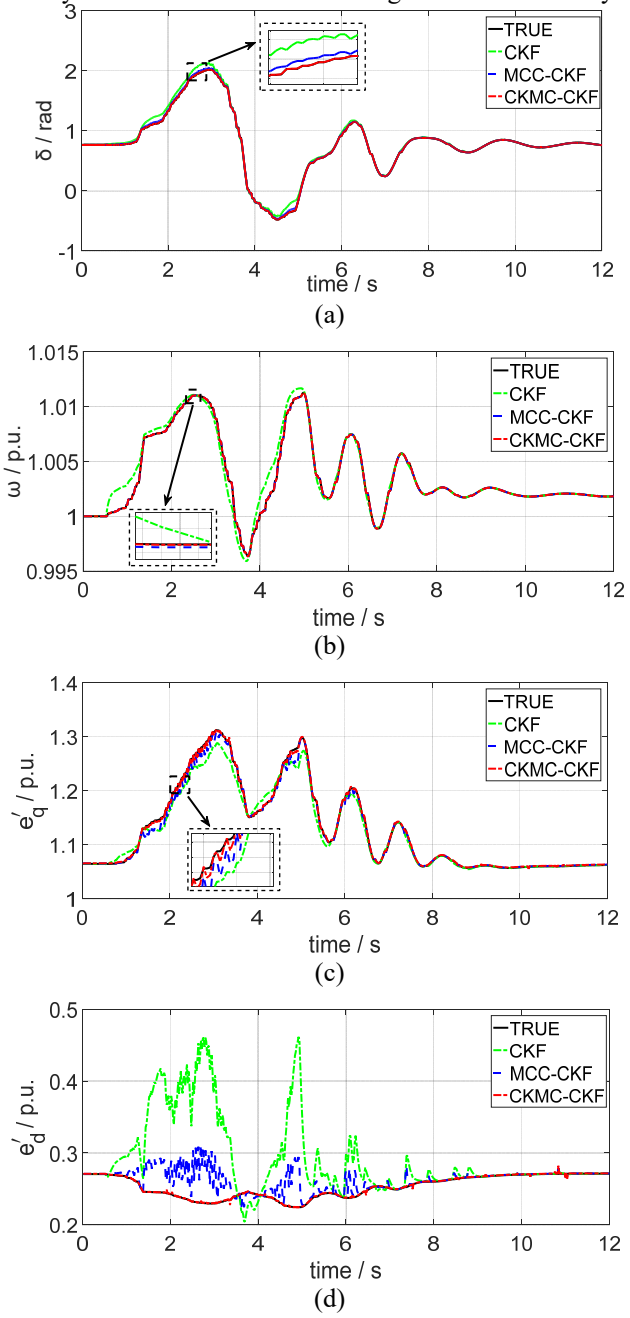

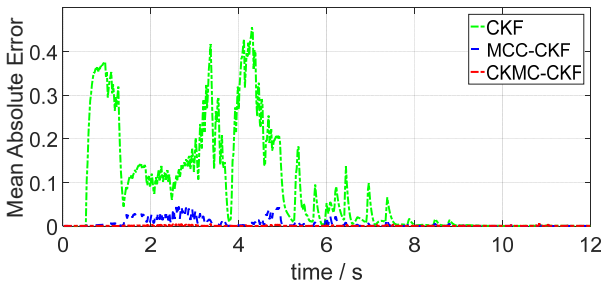

Fig. 2 Estimation performance of the CKF, the MCC-CKF and the CKMC-CKF with non-Gaussian noise. (a) state δ, (b) state ω, (c) state $e_q^{'}$, (d) state $e_d^{'}$, (e) MAE results.

In addition, to further illustrate the effectiveness of the proposed method against non-Gaussian noise, various mixing degrees that presented in TABLE IV-VI are utilized. Among them, the measurement covariance is taken as $v_1=10^{-4}$, $v_2=10^{-6}$, respectively. It can be found that the error index of CKF is the largest, followed by MCC-CKF and CKMC-CKF. That is to say, the developed CKMC-CKF can achieve the best performance. These results further demonstrate the robustness and efficacy of CKMC-CKF against non-Gaussian noise.

TABLE IV
ERROR METRICS OF DIFFERENT METHODS WITH MIXING DEGREES $\theta=0.98$

States	CKF		MCC-CKF		CKMC-CKF	
	O_x	$MAE(k)$	O_x	$MAE(k)$	O_x	$MAE(k)$
δ	0.0088	0.0048	0.0022	0.0012	0.0011	0.0004
ω	0.0663	0.0350	0.0014	0.0008	0.0009	0.0003
$e_q^{'}$	0.0041	0.0025	0.0026	0.0017	0.0023	0.0015
$e_d^{'}$	0.0118	0.0067	0.0038	0.0022	0.0022	0.0009

TABLE V
ERROR METRICS OF DIFFERENT METHODS WITH MIXING DEGREES $\theta=0.95$

States	CKF		MCC-CKF		CKMC-CKF	
	O_x	$MAE(k)$	O_x	$MAE(k)$	O_x	$MAE(k)$
δ	0.0087	0.0046	0.0019	0.0010	0.0003	0.0002
ω	0.0664	0.0351	0.0002	0.0001	0.0002	0.0001
$e_q^{'}$	0.0039	0.0023	0.0025	0.0016	0.0019	0.0014
$e_d^{'}$	0.0117	0.0064	0.0034	0.0018	0.0005	0.0004

TABLE VI
ERROR METRICS OF DIFFERENT METHODS WITH MIXING DEGREES $\theta=0.9$

States	CKF		MCC-CKF		CKMC-CKF	
	O_x	$MAE(k)$	O_x	$MAE(k)$	O_x	$MAE(k)$
δ	0.0087	0.0047	0.0021	0.0011	0.0009	0.0003
ω	0.0663	0.0351	0.0014	0.0008	0.0009	0.0004
$e_q^{'}$	0.0039	0.0024	0.0025	0.0017	0.0022	0.0015
$e_d^{'}$	0.0116	0.0065	0.0036	0.0021	0.0019	0.0008

D. DoS Attacks Test

The actual power system is usually subject to a denial of service (DoS) attacks, which seriously harms the estimation accuracy of DSE [21]. Therefore, to test the resilient of CKMC-CKF, the scenario where the measurements with DoS attacks is taken into account. In order to fully verify the effectiveness of the proposed method under DoS attacks, different packet loss probabilities of measurements in Table VII which caused by the DoS attacks are investigated. Due to the page limited, only the state estimation results of power angle and electrical angular velocity of the synchronous generator 2 are presented, which is embodied in Figs. 3-6.

TABLE VII
PROBABILITY OF PACKET LOSS UNDER DOS ATTACKS

Packet loss scenarios	loss probability (ρ)
Scenario A	$\rho = 0.02$
Scenario B	$\rho = 0.05$
Scenario C	$\rho = 0.1$
Scenario D	$\rho = 0.2$

As we can see from the Figs. 3-6, the traditional CKF performs badly because as a standard Gaussian filter method, it is not able to deal with the outliers caused by DoS attacks. Furthermore, considering its limited inhibition effect on abnormal measurement in the process of measurement loss, the MCC-CKF method is also powerless against incomplete measurement information that caused by the DoS attacks. In contrast, the proposed CKMC-CKF always outperforms the other discussed methods, because the Cauchy kernel can effectively reduce the weight of outliers and maintain non-singularity during matrix factorization. These estimation results demonstrated the resilient of CKMC-CKF against DoS attacks.

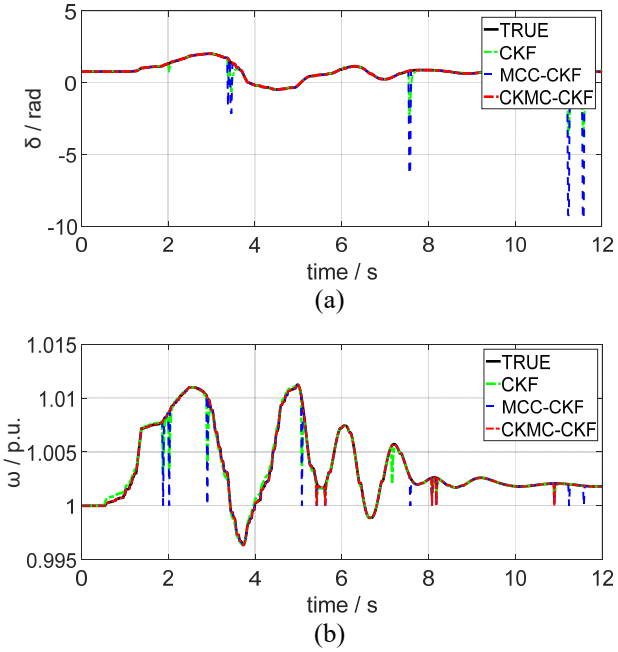

Fig. 3 Estimation performance of the CKF, the MCC-CKF and the CKMC-CKF under scenario A: (a) state variable δ, (b) state variable ω.

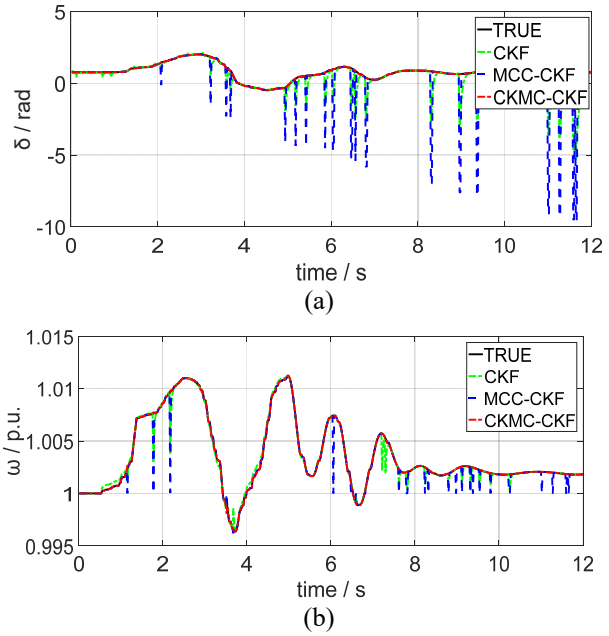

Fig. 4 Estimation performance of the CKF, the MCC-CKF and the CKMC-CKF under scenario B: (a) state variable δ, (b) state variable ω.

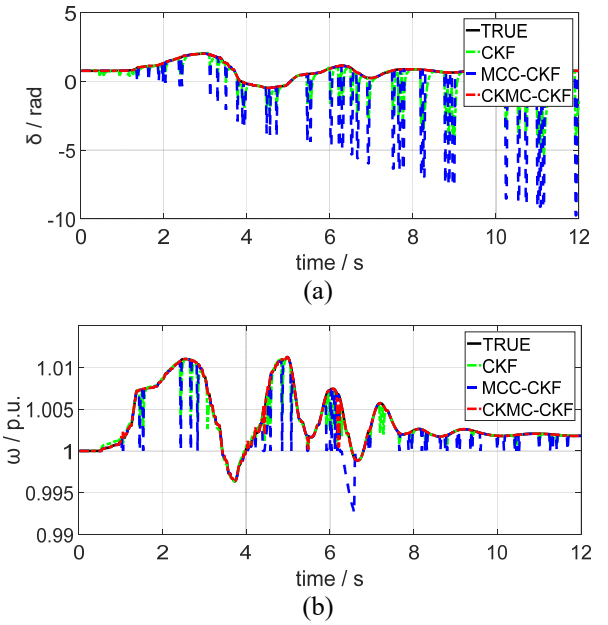

Fig. 5 Estimation performance of the CKF, the MCC-CKF and the CKMC-CKF under scenario C: (a) state variable δ, (b) state variable ω.

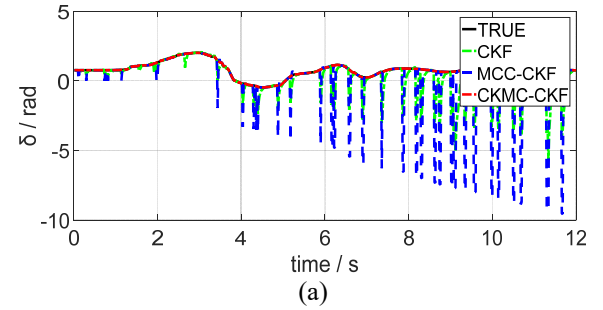

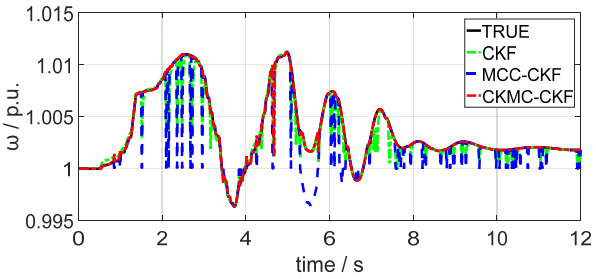

(b)

Fig. 6 Estimation performance of the CKF, the MCC-CKF and the CKMC-CKF under scenario D: (a) state variable δ. (b) state variable ω.

E. Observation Outliers Test

In view of the imperfect measurement synchronization, the saturation of the measurement current transformers, etc., the observation signals collected by the PMU may cause sudden changes [31].

In order to further verify the robustness of various filters, it is assumed that there is a 20% deviation error for the real and reactive powers of G2 when the fault occurs during 6.0s - 6.2s. The tracking effect of different filters is shown in Figure 7, and it can be seen from it that the CKF estimation results rapidly deviate from the true value due to its lack of robustness against observation mutations. Simultaneously, the MCC-CKF method also has a large deviation and cannot suppress the outliers in the observation. In contrast, the CKMC-CKF can minimize the weight of anomaly measurements by using two locally similar functions, so its estimation accuracy is the highest.

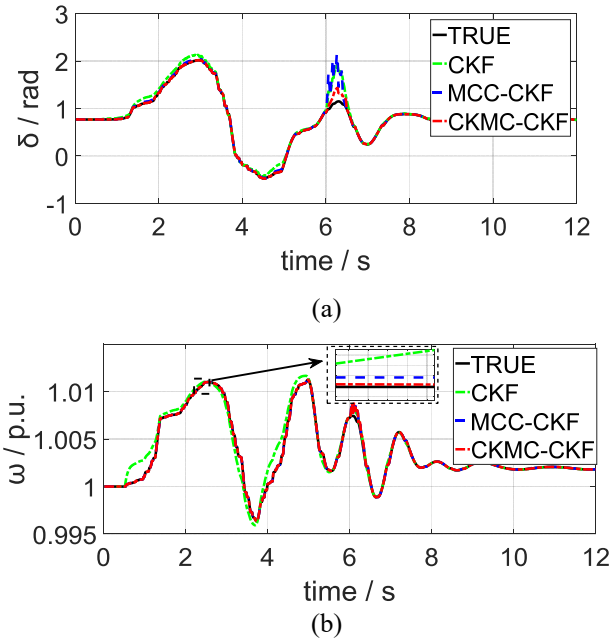

(a)

(b)

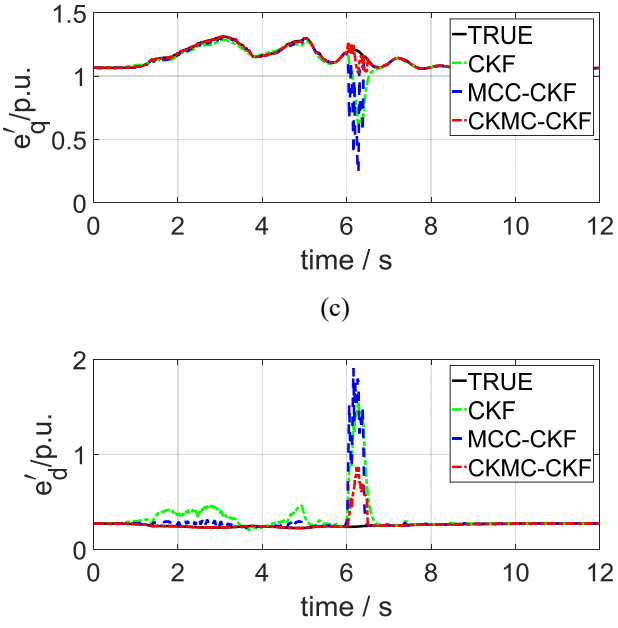

(c)

(d)

Fig. 7 Estimation performance of the CKF, the MCC-CKF and the CKMC-CKF with observation outliers. (a) state δ, (b) state ω, (c) state $e_q^{'}$, (d) state $e_d^{'}$.

F. Execution Time Test

In order to verify the possibility of real-time online application of the developed method, the computational efficiency of all the discussed approaches under the cases of subsections *B*, *C* ($\theta = 0.9$), *D* (with $\rho = 0.01$) and *E* are investigated in detail. To be specific, the total execution time of the standard CKF, MCC-CKF and the proposed CKMC-CKF method under different scenarios is shown in Fig. 8. As we can see from the Fig. 8, the standard CKF takes the least calculation time, followed by MCC-CKF and CKMC-CKF. That is to say, the proposed CKMC-CKF takes a bit more computational effort than the conventional methods. This is because the calculation of correntropy gain increased the complexity. Nonetheless, it still meets the sampling (20ms, 50 samples/sec) requirements of the PMU.

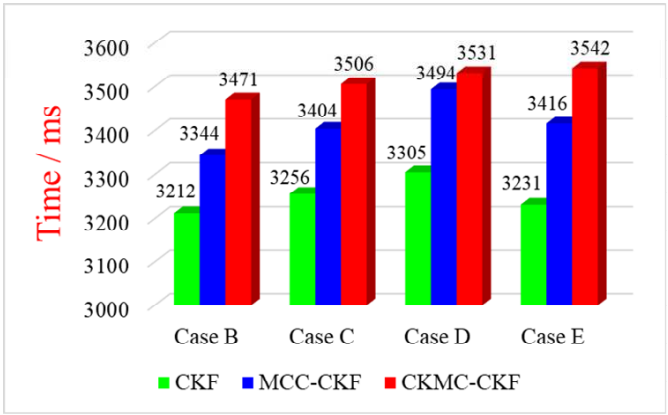

Fig. 8 Total execution time of different DSE methods for cases B-E

V. Conclusion

In this paper, a novel resilient approach termed CKMC-CKF was developed for power system dynamic state estimation against the inevitable non-Gaussian noise and randomly occurring denial-of-service (DoS) attacks. In which, both the statistical linearization strategy and fixed-point iterative approach were introduced to acquire the optimal estimation. Moreover, the Cauchy kernel maximum correntropy, which was utilized to describe the distance between vectors, enhanced the state estimation performance of the DSE method. Extensive simulation experiments carried out on the standard IEEE 39-bus system under various abnormal conditions demonstrated and confirmed that the proposed method can achieve the best estimation performance and robustness compared with the traditional CKF and MCC-CKF.

References

[1] C. Muscas, P. A. Pegoraro, S. Sulis, M. Pau, F. Ponci, and A. Monti, "New Kalman filter approach exploiting frequency knowledge for accurate PMU-based power system state estimation," *IEEE Trans. Instrum. Meas*., vol. 69, no. 9, pp. 6713–6722, Sep. 2020.

[2] M. Ahwiadi and W. Wang, "An adaptive particle filter technique for system state estimation and prognosis," *IEEE Trans. Instrum. Meas*., vol. 69, no. 9, pp. 6756–6765, Sep. 2020.

[3] R. Ferrero, P. A. Pegoraro, and S. Toscani, "Dynamic synchrophasor estimation by extended Kalman filter," *IEEE Trans. Instrum. Meas*., vol. 69, no. 7, pp. 4818–4826, Jul. 2020.

[4] D. Hou, Y. Sun, J. Wang, L. Zhang, and S. Wang, "Dynamic state estimation of power systems with uncertainties based on a robust adaptive unscented Kalman filter," *J. Mod. Power Syst. Clean Energy*, doi: 10.35833/MPCE.2022.000157.

[5] L. Chen, Y. Li, M. Huang, X. Hui, and S. Gu, "Robust dynamic state estimator of integrated energy systems based on natural gas partial differential equations," *IEEE Trans. Ind. Appl.*, vol. 58, no. 3, pp. 3303-3312, May 2022.

[6] D. Ćetenovića, A. Ranković, J. Zhao, Z. Jin, J. Wu, and V. Terzija, "An adaptive method for tuning process noise covariance matrix in EKF-based three-phase distribution system state estimation," *Int. J. Electr. Power Energy Syst.*, vol. 132, pp. 107192, Nov. 2022.

[7] C. Mishra, L. Vanfretti, and K. D. Jones, "Synchrophasor phase angle data unwrapping using an unscented Kalman filter," *IEEE Trans. Power Syst.*, vol. 36, no. 5, pp. 4868-4871, Sep. 2021.

[8] Z. Li, S. Li, B. Liu, S. S. Yu, and P. Shi, "A stochastic event-triggered robust cubature Kalman filtering approach to power system dynamic state estimation with non-Gaussian measurement noises," *IEEE Trans. Control Syst. Technol.*, doi: 10.1109/TCST.2022.3184467.

[9] H. Fang, M. A. Haile, and Y. Wang, "Robust extended Kalman filtering for systems with measurement outliers," *IEEE Trans. Control Syst. Technol.*, vol. 30, no. 2, pp. 795-802, Mar. 2022.

[10] Y. Wang, Z. Yang, Y. Wang, V. Dinavahi, J. Liang, and K. Wang, "Robust dynamic state estimation for power system based on adaptive cubature Kalman filter with generalized correntropy loss," *IEEE Trans. Instrum. Meas.,* vol. 71, pp. 1-11, 2022.

[11] V. Mahshad and R.S. Luis, "Abridged Gaussian sum extended Kalman filter for nonlinear state estimation under non-Gaussian process uncertainties." *Comput. Chem. Eng.,* vol. 155, pp. 107534, 2021.

[12] L. Dang, W. Wang, and B. Chen, "Square root unscented Kalman filter with modified measurement for dynamic state estimation of power systems," *IEEE Trans. Instrum. Meas.,* vol. 71, pp. 1-13, May 2022.

[13] K. Jiang, H. Zhang, H. R. Karimi, J. Lin, and L. Song, "Simultaneous input and state estimation for integrated motor-transmission systems in a controller area network environment via an adaptive unscented Kalman filter," *IEEE Trans. Syst. Man Cybern. Syst.*, vol. 50, no. 4, pp. 1570-1579, Apr. 2020.

[14] Y. Lv and G. Yang, "An adaptive cubature Kalman filter for nonlinear systems against randomly occurring injection attacks," *Appl. Math. Comput.,* 2022, 418: 126834.

[15] H. Zhao and B.Tian, "Robust power system forecasting-aided state estimation with generalized maximum mixture correntropy unscented Kalman filter," *IEEE Trans. Instrum. Meas.,* vol. 71, pp. 1-10, 2022, Art no. 9002610.

[16] Y. Zhang, C. Peng, S. Xie, and X. Du, "Deterministic network calculus-based H∞ load frequency control of multiarea power systems under malicious DoS attacks," *IEEE Trans. Smart Grid,* vol. 13, no. 2, pp. 1542-1554, Mar. 2022.

[17] W. Chen, D. Ding, and H. Dong, "Distributed resilient filtering for power systems subject to denial-of-service attacks," *IEEE Trans. Syst. Man Cybern. -Syst.*, vol. 13, no.2, pp. 1542-1554, Apr. 2019.

[18] B. Rout and B. Natarajan, "Impact of cyber attacks on distributed compressive sensing based state estimation in power distribution grids," *Int. J. Electr. Power Energy Syst.*, vol. 142, pp. 108295, Nov. 2022.

[19] X. Liu, Z. Ren, H. Lyu, Z. Jiang, P. Ren, and B. Chen, "Linear and nonlinear regression-based maximum correntropy extended Kalman filtering," *IEEE Trans. Syst. Man Cybern. -Syst.,* vol. 51, no. 5, pp. 3093-3102, May 2021.

[20] W. Ma, J. Qiu, X. Liu, G. Xiao, J. Duan, and B. Chen, "Unscented Kalman filter with generalized correntropy loss for robust power system forecasting-aided state estimation," *IEEE Trans. Ind. Inform.,* vol. 15, no. 11, pp. 6091-6100, Nov. 2019.

[21] Song H, Ding D, and Dong H, "Distributed filtering based on Cauchy-kernel-based maximum correntropy subject to randomly occurring cyber-attacks," *Automatica*, vol. 135, pp. 110004, 2022.

[22] J. He, C. Sun, B. Zhang, and P. Wang, "Variational Bayesian-based maximum correntropy cubature Kalman filter with both adaptivity and robustness," *IEEE Sens. J.*, vol. 21, no. 2, pp. 1982-1992, Jan. 2021.

[23] J. Zhao and L. Mili, "A decentralized H-infinity unscented Kalman filter for dynamic state estimation against uncertainties," *IEEE Trans. Smart Grid,* vol. 10, no. 5, pp. 4870-4880, Sep. 2019.

[24] G. Cheng, Y. Lin, J. Zhao, and J. Yan, "A highly discriminative detector against false data injection attacks in AC state estimation," *IEEE Trans. Smart Grid,* vol. 13, no. 3, pp. 2318-2330, May 2022.

[25] H. Alhelou and P. Cuffe, "Dynamic-state-estimator-based tolerance control method against cyber attacks and erroneous measured data for power systems," *IEEE Trans. Ind. Inform.,* vol. 18, no.7, pp. 4990-4999, Jun. 2021.

[26] Q. Su, H. Wang, and C. Sun, "Cyber-attacks against cyber-physical power systems security: state estimation, attacks reconstruction and defense strategy," *Appl. Math. Comput.,* vol. 413, pp: 126639, 2022.

[27] S. Fakoorian, A. Santamaria-Navarro, B. T. Lopez, D. Simon, and A. Agha-mohammadi, "Towards robust state estimation by boosting the maximum correntropy criterion Kalman filter with adaptive behaviors," *IEEE Robot. Autom. Let.,* vol. 6, no. 3, pp. 5469-5476, Jul. 2021.

[28] Q. Meng and X. Li, "Minimum Cauchy kernel loss based robust cubature Kalman filter and its low complexity cost version with application on INS/OD integrated navigation system," *IEEE Sens. J.*, vol. 22, no. 10, pp. 9534-9542, May 2022.

[29] S. Li, B. Xu, and L. Wang, "Improved maximum correntropy cubature Kalman filter for cooperative localization," *IEEE Sens. J.*, vol. 20, no. 22, pp. 13585-13595, Jun. 2019.

[30] Y. Sun, Y. Wang, V. Dinavahi, K. Wang, and D. Nan, "Robust dynamic state estimation of power systems with model uncertainties based on adaptive unscented H∞ filter," *IET Gener. Transm. Dis*., vol. 13, no. 12, pp. 2455-2463, 2019.

[31] J. Zhao and L. Mili. "A theoretical framework of robust H-infinity unscented Kalman filter and its application to power system dynamic state estimation," *IEEE Trans. Signal Process*., vol. 67, no. 10, pp. 2734-2746, 2019.

Yi Wang (Member, IEEE) received his B.S. degree from Luoyang Institute of Science and Technology, Luoyang, China, in 2014; and received his Ph.D. degrees from Hohai University, Nanjing, China, in 2020.

He was a visiting scholar at the University of Alberta between 2018 and 2019. His current research interests include theoretical and algorithmic studies in power system estimation, parameters identification, power system dynamics, signal processing, and cyber security. He is also an active reviewer

for many international journals.

Zhiwei Yang (Student Member, IEEE) received his B.S. degree in Electric Power System & its Automation from Henan University of Technology, Zhengzhou, China, in 2019. He is currently pursuing the M.S. degree in Electrical Engineering at Zhengzhou University, Zhengzhou, China. His research interests include theoretical and algorithmic studies in power system estimation.

Yaoqiang Wang (Senior Member, IEEE & CSEE) received his B.S. degree from Hangzhou Dianzi University, Hangzhou, China, in 2006; and his M.S. and Ph.D. degrees from the Harbin Institute of Technology, Harbin, China, in 2008 and 2013, respectively.

He is currently a Professor with the School of Electrical and Information Engineering, Zhengzhou University, Zhengzhou, China. He is also serving as the Director of the Henan Provincial Engineering Research Center of Power Electronics and Energy Systems (HERC-PEES). He has authored more than 60 technical papers including over 50 journal papers, and is the holder of more than 20 patents. His current research interests include power electronics and electrical drives, renewable power generation, new energy power system, power system operation and control.

Zhongwen Li (Member, IEEE) received his B.S. degree in Control Science and Engineering from Zhengzhou University, Zhengzhou, China, in 2011, and the Ph.D. degree in Control Theory and Control Engineering from Shenyang Institute of Automation, Chinese Academy of Sciences, Shenyang, China, in 2017.

He is currently an associate professor at Zhengzhou University. His main research interests include distributed control, power systems, renewable energy systems, and AGC.

Venkata Dinavahi (Fellow, IEEE) received the B.Eng. degree in electrical engineering from Visvesvaraya National Institute of Technology (VNIT), Nagpur, India, in 1993, the M.Tech. degree in electrical engineering from the Indian Institute of Technology (IIT) Kanpur, India, in 1996, and the Ph.D. degree in electrical and computer engineering from the University of Toronto, Ontario, Canada, in 2000.

He is currently a Professor with the Department of Electrical and Computer Engineering, University of Alberta, Edmonton, Alberta, Canada. He is a Fellow of the Engineering Institute of Canada. His research interests include real-time simulation of power systems and power electronic systems, electromagnetic transients, device level modeling, large-scale systems, and parallel and distributed computing.

Jun Liang (Senior Member, IEEE) received his B.S. degree in Electric Power System & its Automation from the Huazhong University of Science and Technology, Wuhan, China, in 1992; and his M.S. and Ph.D. degrees in Electric Power System & its Automation from the China Electric Power Research Institute (CEPRI), Beijing, in 1995 and 1998, respectively.

From 1998 to 2001, he was a Senior Engineer with CEPRI. From 2001 to 2005, he was a Research Associate with Imperial College London, U.K. From 2005 to 2007, he was with the University of Glamorgan, Pantiplife, U.K., as a Senior Lecturer. He is currently a Professor in Power Electronics with the School of Engineering, Cardiff University, Cardiff, U.K. He is the Coordinator and Scientist-in-Charge of two European Commission Marie-Curie Action ITN/ETN projects: MEDOW (€3.9M) and InnoDC (€3.9M). His research interests include HVDC, MVDC, FACTS, power system stability control, power electronics, and renewable power generation.

Prof. Liang is a Fellow of the Institution of Engineering and Technology (IET). He is the Chair of IEEE UK and Ireland Power Electronics Chapter. He is an Editorial Board Member of CSEE JPES. He is an Editor of the IEEE Transactions on Sustainable Energy.